

# Untangling the Formation of Methoxymethanol (CH<sub>3</sub>OCH<sub>2</sub>OH) and Dimethyl Peroxide (CH<sub>3</sub>OOCH<sub>3</sub>) in Star-forming Regions

Cheng Zhu<sup>1,2</sup>, Robert Frigge<sup>1,2</sup>, Alexandre Bergantini<sup>1,2</sup>, Ryan C. Fortenberry<sup>3</sup>, and Ralf I. Kaiser<sup>1,2</sup>, Department of Chemistry, University of Hawaii at Mānoa, Honolulu, HI 96822, USA; r410@olemiss.edu, ralfk@hawaii.edu

<sup>2</sup> W.M. Keck Laboratory in Astrochemistry, University of Hawaii at Mānoa, Honolulu, HI 96822, USA

<sup>3</sup> Department of Chemistry & Biochemistry, University of Mississippi, University, MS 38677-1848, USA

\*\*Received 2019 January 23; revised 2019 June 10; accepted 2019 June 11; published 2019 August 22

#### **Abstract**

Methoxymethanol (CH<sub>3</sub>OCH<sub>2</sub>OH) was recently detected toward the MM1 core in the high-mass star-forming region NGC 6334I. However, the underlying formation mechanisms of this complex organic molecule (COM) as well as its structural isomers ethylene glycol (HOCH<sub>2</sub>CH<sub>2</sub>OH) and the hitherto unobserved dimethyl peroxide (CH<sub>3</sub>OOCH<sub>3</sub>) are still elusive. Here, we report the very first confirmed synthesis of dimethyl peroxide—at various deuteration levels within interstellar analogous ices of D<sub>3</sub>-methanol (CD<sub>3</sub>OH) exposed to ionizing radiation at ultralow temperatures of 5 K. The discrimination of specific isomers is achieved by exploiting reflectron time-of-flight mass spectrometry coupled with isomer-selective photoionization of the subliming molecules in the temperature programmed desorption phase of the experiment. Based on the distribution of the identified species at distinct mass-to-charge ratios, we reveal primary and secondary reaction pathways to methoxymethanol, ethylene glycol, and dimethyl peroxide involving radical–radical recombination of methoxy (CH<sub>3</sub>O) and hydroxymethyl (CH<sub>2</sub>OH). Our findings help to constrain the formation mechanism of COMs detected within star-forming regions (methoxymethanol, ethylene glycol) and propose that the hitherto elusive dimethyl peroxide isomer represents an excellent candidate for future astronomical searches.

Key words: astrochemistry – cosmic rays – ISM: molecules – methods: laboratory: solid state – molecular processes – radiation mechanisms: non-thermal

#### 1. Introduction

During the last decade, structural isomers—molecules with the same molecular formula but different connectivities of atoms—have emerged as tracers in constraining the chemical and physical conditions of distinct interstellar environments, such as cold molecular clouds and star-forming regions (Turner 1971; Snyder et al. 1974; Brown et al. 1975; Gilmore et al. 1976; Kawaguchi et al. 1992b; Howe et al. 1994; Mehringer et al. 1997; Turner & Apponi 2001; Laas et al. 2011; Neill et al. 2012; Loomis et al. 2015; Loison et al. 2016; Xue et al. 2019). For instance, the isomer family C<sub>3</sub>NH consisting of cyanoacetylene (HCCCN; Turner 1971; Howe et al. 1994), isocyanoacetylene-1 (HCCNC; Kawaguchi et al. 1992a), and isocyanoacetylene-2 (HNCCC; Kawaguchi et al. 1992b) as detected in TMC-1 served as a benchmark to highlight the critical role of gas-phase neutral-neutral versus ion-molecule reactions in the formation of cyanopolyvnes and of cyanoacetylene in particular (Huang et al. 1999, 2000). Structural isomers have also been exploited to decipher reaction mechanisms synthesizing C<sub>2</sub>H<sub>4</sub>O (Bennett et al. 2005a, 2005b), C<sub>2</sub>H<sub>4</sub>O<sub>2</sub> (Bennett & Kaiser 2007a, 2007b; Maity et al. 2014; Bergantini et al. 2018b), and C<sub>2</sub>H<sub>6</sub>O (Bergantini et al. 2017, 2018a) isomers (Scheme 1) via galactic cosmic-ray (GCR) mediated nonequilibrium chemistry, highlighting the role of ice bulk chemistry.

The recent detection of methoxymethanol (CH<sub>3</sub>OCH<sub>2</sub>OH; McGuire et al. 2017)—an isomer of the well-known ethylene glycol (HOCH<sub>2</sub>CH<sub>2</sub>OH) and the still elusive dimethyl peroxide (CH<sub>3</sub>OOCH<sub>3</sub>)—toward the MM1 core in the high-mass star-forming region NGC 6334I with column density of (4  $\pm$  2)  $\times$   $10^{18}\,\mathrm{cm}^{-2}$  using the Atacama Large Millimeter/submillimeter Array raises fundamental questions about the mechanistical

processes taking place during the formation of such complex organic molecules (COMs) in the interstellar medium (ISM). Gas phase ion-molecule association reactions followed by dissociative recombination processes are unlikely to be dominant formation mechanisms (McGuire et al. 2017) as several constraints (well depths of reaction intermediates of a few eV), reactants size (more than 4–5 atoms), and temperatures (<100 K) likely limit the rates of the reaction. McGuire et al. (2017) speculated that CH<sub>3</sub>OCH<sub>2</sub>OH can be generated via successive hydrogenation of precursor species on grain surfaces

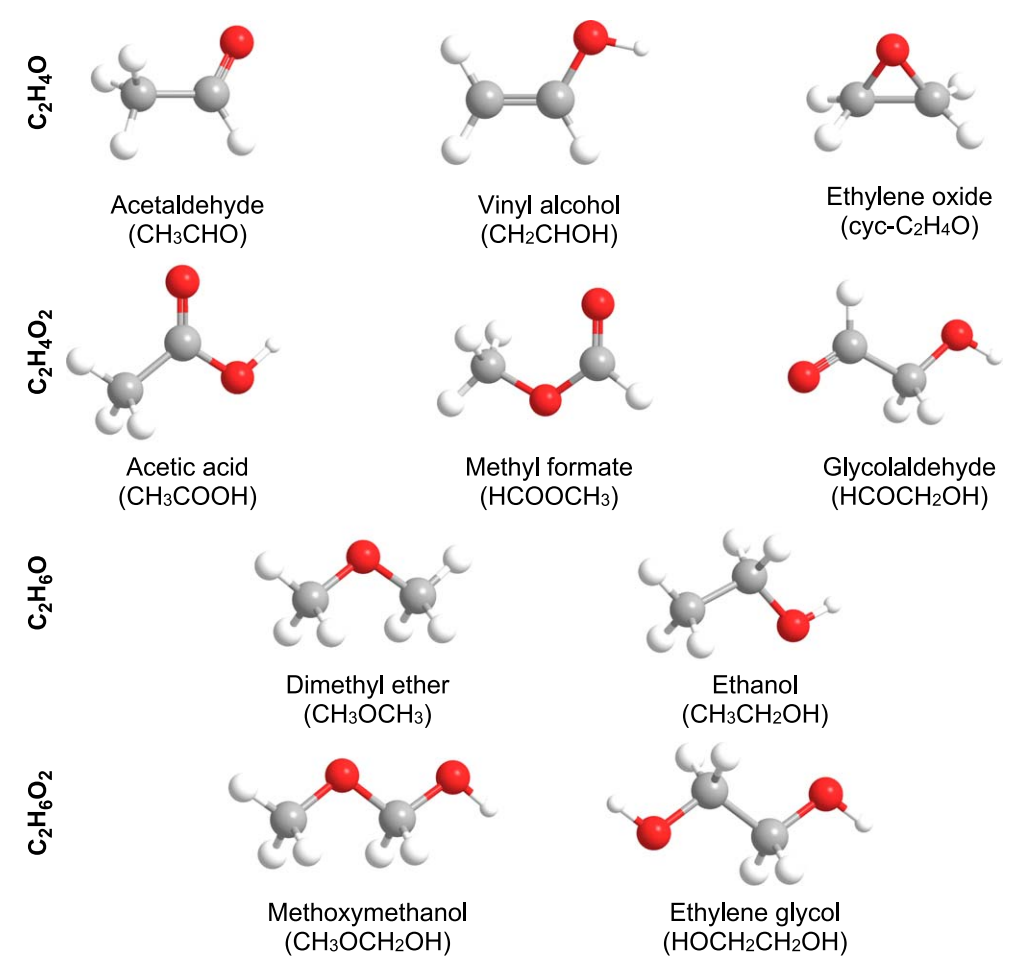
$$CH_3OCHO + H \rightarrow CH_3OCHOH$$
 (1)

$$CH_3OCHOH + H \rightarrow CH_3OCH_2OH.$$
 (2)

Hays & Widicus Weaver studied theoretically the possible formation of CH<sub>3</sub>OCH<sub>2</sub>OH via insertion of electronically excited oxygen atoms O(<sup>1</sup>D) into one of the C–H bonds of CH<sub>3</sub>OCH<sub>3</sub> in the gas phase (Hays & Widicus Weaver 2013)

$$CH_3OCH_3 + O(^1D) \rightarrow CH_3OCH_2OH.$$
 (3)

O(¹D) can be generated in dust-grain ice mantles by GCRs (Bennett et al. 2010). This reaction could occur efficiently in interstellar ices, but is unlikely in the gas phase (especially low-density environments) as the excited species radiatively relaxes before colliding with a reaction partner. Also, bimolecular reactions dominate gas phase reactions, whereas termolecular reactions are absent. Several laboratory studies detected C<sub>3</sub>H<sub>6</sub>O<sub>2</sub> isomer(s) in interstellar analogous ices containing methanol (CH<sub>3</sub>OH) exposed to electrons and photons (Harris et al. 1995; Boamah et al. 2014; Maity et al. 2015; Sullivan et al. 2016; Bergantini et al. 2017; Schneider et al. 2019). The proposed



Scheme 1. Detected C<sub>2</sub>H<sub>4</sub>O, C<sub>2</sub>H<sub>4</sub>O<sub>2</sub>, C<sub>2</sub>H<sub>6</sub>O, and C<sub>2</sub>H<sub>6</sub>O<sub>2</sub> isomers in the ISM.

formation pathways and the nature of the isomer formed include cleavage of the oxygen–hydrogen (reaction 4) or carbon–hydrogen bonds (reactions (5)) of methanol (CH $_3$ OH) followed by recombination of the methoxy (CH $_3$ O) and hydroxymethyl (CH $_2$ OH) radicals (reaction 6; Boyer et al. 2014)

$$CH_3OH \rightarrow CH_3O + H$$
 (4)

$$CH_3OH \rightarrow CH_2OH + H$$
 (5)

$$CH_3O + CH_2OH \rightarrow CH_3OCH_2OH.$$
 (6)

Here, we report unambiguous synthesis and detection of methoxymethanol as well as its isomers dimethyl peroxide and ethylene glycol (Scheme 1) in interstellar analogous ices of methanol exposed to ionizing radiation in the form of energetic electrons simulating secondary electrons released while GCRs penetrate interstellar ices (Bennett et al. 2005a). The confirmed detection of the three isomers is achieved using fragment-free tunable vacuum ultraviolet (VUV) photoionization reflectron time-of-flight mass spectrometry (PI-ReTOF-MS), which has been demonstrated to be able to selectively discriminate between structural isomers of molecules by employing distinct photon energies based on the ionization energies (IE) of these organic molecules (Abplanalp et al. 2016b; Frigge et al. 2018; Turner et al. 2018; Zhu et al. 2018). Furthermore, with partially deuterated precursor D<sub>3</sub>-methanol (CD<sub>3</sub>OH), we reveal primary and secondary formation pathways of CH<sub>3</sub>OCH<sub>2</sub>OH, HOCH<sub>2</sub>CH<sub>2</sub>OH, and CH<sub>3</sub>OOCH<sub>3</sub> through recombination of methoxy (CH<sub>3</sub>O) and hydroxymethyl (CH<sub>2</sub>OH) radicals. Methanol was first detected toward Sagittarius A and Sagittarius B2 (Ball et al. 1970) and has been found to be ubiquitous in the ISM at a level up to 30%, compared to water in interstellar ices (Boogert et al. 2008, 2015). Our results represent a significant advance in the understanding of formation pathways of distinct  $C_2H_6O_2$  isomers found in the ISM and help to constrain astrochemical models and grain bulk ice chemistry on the formation of such species. Finally, we predict that the hitherto undetected dimethyl peroxide (CH<sub>3</sub>OOCH<sub>3</sub>) isomer is likely present in star-forming regions, since its isomers have been detected in molecular clouds and hot cores (Hollis et al. 2002; Brouillet et al. 2015; McGuire et al. 2017), and all three structural isomers are formed in the laboratory simulation experiments.

## 2. Experimental Methods

The experiments were performed at the W. M. Keck Research Laboratory in Astrochemistry (Jones & Kaiser 2013; Abplanalp et al. 2016a, 2016b). The experimental setup consists of a contamination-free stainless steel ultra-high vacuum chamber (UHV) evacuated to a base pressure of a few 10<sup>-11</sup> Torr by magnetically levitated turbo molecular pumps coupled to oil-free scroll backing pumps. Within the chamber, a silver mirror substrate is interfaced to a cold finger, which is connected to a closed cycle helium compressor (Sumitomo Heavy Industries,

 Table 1

 Parameters for the Vacuum Ultraviolet Light Generation Used in the Present Experiments<sup>a</sup>

$2\omega_1-\omega_2$	Photoionization Energy (eV)	$10.49 (3\omega_1)$	10.20	9.40	9.00
	Flux (10 <sup>11</sup> photons s <sup>-1</sup> )	12 ± 1	10 ± 1	10 ± 1	10 ± 1
	Wavelength (nm)	118.22	121.55	131.90	137.76
$\omega_1$	Wavelength (nm)	355	202.316	222.566	222.566
Nd:YAG (YAG A)	Wavelength (nm)	355	532	355	355
Dye laser (DYE A)	Wavelength (nm)		606.948	445.132	445.132
Dye			Rh 610/Rh 640	C450	C450
$\omega_2$	Wavelength (nm)	•••	603	712	579
Nd:YAG (YAG B)	Wavelength (nm)	•••	532	532	532
Dye laser (DYE B)	Wavelength (nm)		603	712	579
Dye			Rh 610/Rh 640	Pyridine 2	Pyrromethene 597
	Nonlinear medium	Xe	Kr	Xe	Xe

#### Note.

RDK-415E) capable of reaching  $5.0 \pm 0.1$  K. By utilizing a doubly differentially pumped rotational feedthrough (Thermionics Vacuum Products, RNN-600/FA/MCO) and an UHV compatible bellow (McAllister, BLT106), the substrate is able to be rotated in the horizontal plane and to be translated vertically, respectively. After the substrate was cooled to  $5.0 \pm 0.1 \,\mathrm{K}$ , methanol-D3 (CD<sub>3</sub>OH, Sigma-Aldrich, 99.8 atom % D) was deposited onto the substrate via a precision leak value and glass capillary array for 6 minutes at a pressure of  $2 \times 10^{-8}$  Torr in the main chamber. The growth of the ice was monitored online and in situ via laser interferometry with a helium–neon (He–Ne) laser operating at 632.8 nm (CVI Melles-Griot, 25-LHP-230; Groner et al. 1973; Turner et al. 2015). The light from the laser was reflected to a photodiode (Thorlabs, SM1PD1A) at an angle of 4° relative to the ice surface normal. With the refractive index for solid methanol of  $n_{\text{CH3OH}} = 1.33 \pm 0.04$  (Bouilloud et al. 2015), the ice thickness was determined to be 480  $\pm$  30 nm.

The ices were then isothermally irradiated at  $5.0 \pm 0.1$  K for 60 minutes with 5 keV electrons from an electron gun (Specs, EQ 22-35) at a beam current of 15  $\pm$  1 nA. The electrons were introduced at an angle of 70° relative to the surface normal of the target (1.0  $\pm$  0.1 cm<sup>2</sup>). CASINO 2.42 software (Drouin et al. 2007) was exploited to model the electron trajectories and energy transfer inside the ices. With the density of methanol ice  $\rho = 1.01 \pm 0.03 \text{ g cm}^{-3}$  (Bouilloud et al. 2015), the average penetration depth of the electrons was calculated to be  $250 \pm 30$  nm, which is less than the thickness of the deposited ice (480  $\pm$  30 nm) ensuring no interaction between the electrons and the silver mirror. The averaged dose was determined to be  $2.8 \pm 0.4 \,\mathrm{eV}$  molecule<sup>-1</sup>. During the irradiation, the chemical evolution of the ices was monitored online and in situ using a Fourier transform infrared (FTIR) spectrometer (Nicolet, 6700) from 6000 to 500 cm<sup>-1</sup> with a resolution of 4 cm<sup>-</sup>

After the irradiation, the sample was held at 5.0 K for additional 30 minutes and then warmed up to 300 K at a rate of 0.5 K minute<sup>-1</sup> (temperature programmed desorption; TPD).

The subliming neutral molecules during the TPD phase were selectively ionized by pulsed tunable VUV light at 30 Hz based on their PI energy. The produced ions were mass-resolved and detected utilizing a modified ReTOF mass spectrometer (Jordan TOF products, Inc.) where the arrival time of the ions to a multichannel plate in a dual chevron configuration is based on mass-to-charge ratios. The detected signal was then amplified by a fast preamplifier (Ortec, 9306), shaped with a 100 MHz discriminator (Advanced Research Instruments Corp., F-100T), and recorded using a computer-controlled multichannel scaler (FAST ComTec, P7888-1E) triggered via a pulse delay generator (Quantum Composer, 9518) at 30 Hz. Each ReTOF spectrum was the summation of 3600 sweeps of the mass spectrum in 4 ns bin widths, which corresponds to an increase in the substrate temperature of 1 K.

The VUV light was generated by difference four wave mixing ( $\omega_{\rm vuv} = 2\omega_1 - \omega_2$ ) in a nonlinear medium (krypton (Kr) or xenon (Xe)) using two dye lasers (Sirah Lasertechnik, Models Cobra-Stretch, and Precision Scan) each pumped with a neodymium-doped yttrium aluminum garnet laser (Nd:YAG, Spectra Physics, Models PRO-270-30, and PRO-250-30). The generated VUV light was monitored using a Faraday cup and a silicon photodiode (Digi-Key, SXUV100) calibrated by the National Institute of Standards and Technology. By tuning the VUV photon energies close to the ionization limit of particular species, molecular ions can be produced without fragmentation (Shu et al. 2006; Wilson et al. 2006; Abplanalp et al. 2016a). In this work, VUV light with energies of 10.49 eV (118.19 nm), 10.20 eV (121.55 nm), 9.40 eV (131.90 nm), and 9.00 eV (137.76 nm; Table 1) was exploited to discriminate structural isomers. The 10.49 eV light was generated via frequency tripling  $(\omega_{vuv} = 3\omega_1)$  of the third harmonic (355 nm) of the fundamental of a Nd:YAG laser (YAG A) in pulsed gas jets of Xe. The 10.20 eV light was produced by combining two laser beams  $\omega_1 = 202.316$  nm and  $\omega_2 = 603$  nm in pulsed jets of Kr as a nonlinear medium for difference four wave mixing

<sup>&</sup>lt;sup>a</sup> The uncertainty for VUV photon energies is 0.01 eV.

 Table 2

 Calculated Adiabatic Ionization Energies and Relative Energies ( $E_{rel}$ ) of the  $C_2H_4O_2$  Isomers

C <sub>2</sub> H <sub>6</sub> O <sub>2</sub> Isomers					
Structure	Name	IE (eV) <sup>a</sup>	$\frac{E_{\rm rel} (kJ)}{(kJ \text{ mol}^{-1})^{b}}$		
	Dimethyl peroxide	9.31	273.51		
Care Pr	1-gauche- Methoxymethanol	10.12	11.29		
	2-gauche- Methoxymethanol	10.03	19.34		
6.0	3-gauche- Methoxymethanol	10.01	21.56		
	1-eclipsed- Methoxymethanol	10.29	11.29		
	2-eclipsed- Methoxymethanol	10.21	19.34		
	3-eclipsed- Methoxymethanol	10.19	21.56		
	gauche-Ethylene glycol	9.76	2.39		
	anti-Ethylene glycol	9.79	0.00		

## Notes.

 $(\omega_{\text{vuv}} = 2\omega_1 - \omega_2)$ . To generate  $\omega_1$ , two  $\beta$ -BaB2O4 (BBO) crystals at 44° and 77° were exploited for frequency tripling of 606.948 nm converted from the second harmonic (532 nm) of YAG A by a dye laser (DYE A) with rhodamine 610/640 dye mixture (0.17/0.04 g L<sup>-1</sup> ethanol). To obtain  $\omega_2$ , a different Nd:YAG laser (YAG B) was used to pump another dye laser (DYE B) with the same dye composition. The 9.40 and 9.00 eV were generated by combining  $\omega_1 = 222.566$  nm with  $\omega_2 = 712$  nm and 579 nm, respectively, in Xe. In these two cases, YAG A was operated at 355 nm to pump DYE A with Coumarin 450 (0.20 g L<sup>-1</sup> ethanol) to achieve 445.132 nm, which underwent a frequency doubling process resulting  $\omega_1$ . YAG B was operated at 532 nm to pump DYE B with pyridine 2 (0.25 g L<sup>-1</sup> ethanol) and pyrromethene 597 (0.16 g L<sup>-1</sup> ethanol) to generate 712 nm and 579 nm, respectively.

### 3. Computational Methods

Geometry optimizations of the desired structures are all undertaken with B3LYP (Yang et al. 1986; Lee et al. 1988;

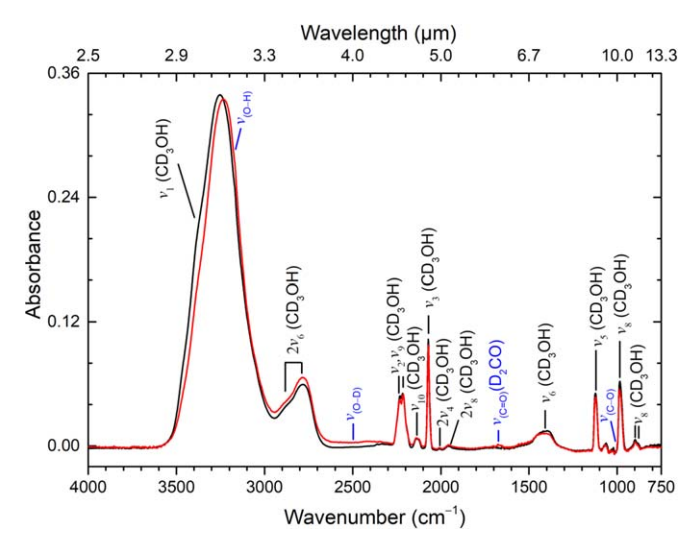


Figure 1. FTIR spectra before (black) and after (red) irradiation of the CD<sub>3</sub>OH ice.

Wavenumb	er (cm <sup>-1</sup> )	Assignment	Reference
Before Irradiation	After Irradiation	<i>G</i>	
3460, 3380, 3250		ν <sub>1</sub> (CD <sub>3</sub> OH)	(1)
	3180	$\nu_{\mathrm{(O-H)}}$	(2)
2875, 2780		$2\nu_6$ (CD <sub>3</sub> OH)	(1)
	2500	$\nu_{ m (O-D)}$	(2)
2233, 2214		$\nu_2$ , $\nu_9$ (CD <sub>3</sub> OH)	(1)
2140		$2\nu_{10}$ (CD <sub>3</sub> OH)	(1)
2070		$\nu_3$ (CD <sub>3</sub> OH)	(1)
2009		$2\nu_4$ (CD <sub>3</sub> OH)	(1)
1958		$2\nu_8$ (CD <sub>3</sub> OH)	(1)
	1672	$\nu_{(C=O)}$ (D <sub>2</sub> CO)	(3)
1414		$\nu_6$ (CD <sub>3</sub> OH)	(1)
1123		$\nu_5$ (CD <sub>3</sub> OH)	(1)
1067, 1033, 1028		$\nu_4, \ \nu_{10} \ (\text{CD}_3\text{OH})$	(1)
	1002	$\nu_{\rm (C-O)}$	(2)
987		$\nu_8$ (CD <sub>3</sub> OH)	(1)
898, 880		$\nu_7$ , $\nu_{11}$ (CD <sub>3</sub> OH)	(1)

**References.** (1) Falk & Whalley (1961), (2) Socrates (2004), (3) Saenko & Feldman (2016).

Becke 1993), the aug-cc-pVTZ basis set (Kendall et al. 1992; Peterson & Dunning 1995) and the Gaussian09 quantum chemistry program (Frisch et al. 2009). Harmonic vibrational frequencies verify the structures as minima and provide the zero-point vibrational energies (ZPVEs) incorporated into the relative energy computations. At each of the optimized structures, coupled cluster singles, doubles, and perturbative triples [CCSD(T)] single-point energies (Raghavachari et al. 1989; Crawford & Schaefer 2000) are computed with both the aug-cc-pVTZ and aug-cc-pVQZ basis sets and the Molpro2015.1 quantum chemistry program (Werner et al. 2012; Werner et al. 2015). These energies are extrapolated for each structure to the complete basis set (CBS) limit via a 2-point formula (Huh & Lee 2003). The most accurate computations reported in this work are subsequently noted as B3LYP/ apVTZ//CCSD(T)/CBS + ZPVE. Relative energies are

<sup>&</sup>lt;sup>a</sup> Relative ionization potential by CCSD(T)/CBS with B3LYP/aug-cc-pVTZ zero-point energy correction in eV.

<sup>&</sup>lt;sup>b</sup> Relative energy by CCSD(T)/CBS with B3LYP/aug-cc-pVTZ zero-point energy correction in kJ mol<sup>-1</sup>.

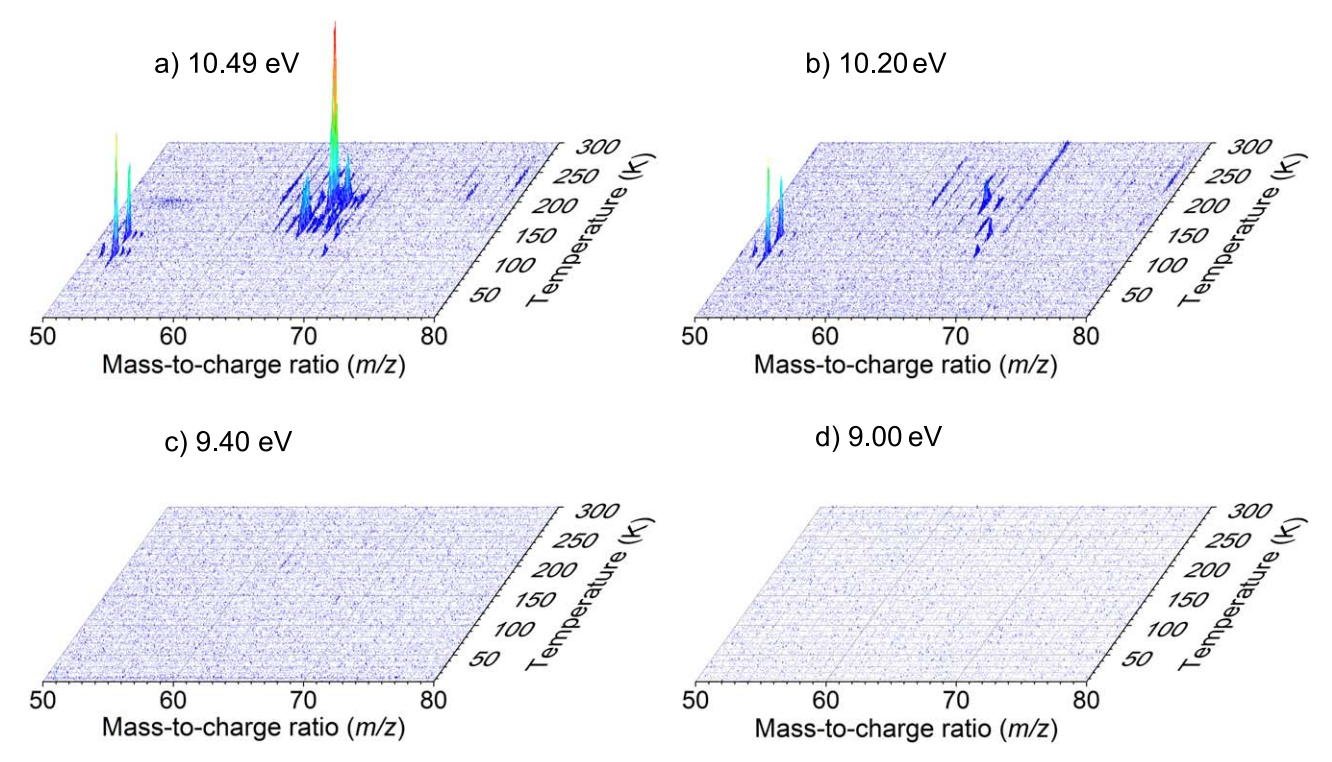


Figure 2. PI-ReTOF-MS spectra of the subliming molecules from irradiated CD<sub>3</sub>OH ices recorded at distinct photon energies.

computed as the differences in these B3LYP/apVTZ//CCSD (T)/CBS + ZPVE energies for the different isomeric or ionized molecular systems within typically 4–8 kJ mol<sup>-1</sup>. Table 2 presents the calculated adiabatic IEs for the C<sub>2</sub>H<sub>6</sub>O<sub>2</sub> isomers along with the relative energies of the structural isomers considered in this study; at this level of theory, the predicted IE are typically within 0.05-0.10 eV of the experiment (Kaiser et al. 2010a, 2010b; Kostko et al. 2010). The reader should note that methoxymethanol has multiple conformers (Hays & Widicus Weaver 2013; Motiyenko et al. 2018). The isomeric numbering for the neutral isomers is as ordered by Hays & Widicus Weaver (2013) while the "eclipsed" and "gauche" names refer to the isomers of the methoxymethanol cations. Additionally, the much larger relative energy for dimethyl peroxide compared to the minimum is a result of the inherently less stable peroxy (-O-O-) bond.

### 4. Results

## 4.1. FTIR

Figure 1 presents the FTIR spectra of a CD<sub>3</sub>OH ice before (black line) and after (red line) the exposure to energetic electrons at 5.0 K. Since the precursor CD<sub>3</sub>OH obscures most of the potential infrared absorptions, the only irradiation induced features are the decomposition of the precursor such as decrease of  $v_1$  at  $3460 \, \mathrm{cm}^{-1}$  and  $v_4$  at  $1414 \, \mathrm{cm}^{-1}$  and a shoulder at  $3180 \, \mathrm{cm}^{-1}$ , a broad absorption in the region of  $2800-2400 \, \mathrm{cm}^{-1}$ , a weak peak at  $1672 \, \mathrm{cm}^{-1}$ , and a shoulder at  $1002 \, \mathrm{cm}^{-1}$ . These can be assigned to stretching modes of oxygen–hydrogen single bond ( $\nu_{(\mathrm{O-D)}}$ ), oxygen–deuterium single bond ( $\nu_{(\mathrm{O-D)}}$ ), carbonyl functional groups ( $\nu_{(\mathrm{C=O)}}$ ) of formaldehyde-D<sub>2</sub> (D<sub>2</sub>CO), and oxygen–carbon single bond ( $\nu_{(\mathrm{C-O)}}$ ), respectively (Table 3; Falk & Whalley 1961; Socrates

2004; Saenko & Feldman 2016). These findings suggest that functional groups (e.g.,  $\nu_{\rm (O-D)}$  and  $\nu_{\rm (C-O)}$ ) linked to deuterated methoxymethanol, dimethyl peroxide, and ethylene glycol can be generated via exposure of CD<sub>3</sub>OH ice to energetic electrons at temperatures as low as 5.0 K. However, since the fundamentals of these isomers fall in similar ranges such as  $\nu_{\rm (O-H)}$  and  $\nu_{\rm (C-O)}$  in the ranges of 3500–3000 cm<sup>-1</sup> and 1100–1000 cm<sup>-1</sup>, respectively (Socrates 2004), infrared spectroscopy does not allow an identification of individual isomers.

## 4.2. PI-ReTOF-MS

To probe discrete molecular species, we exploited PI-ReTOF-MS during the TPD phase of the experiment. Figure 2 compiles the PI-ReTOF-MS data recorded at distinct PI energies of 10.49 eV, 10.20 eV, 9.40 eV, and 9.00 eV, which are selected based on the calculated IEs of the  $C_2H_6O_2$  isomers (Table 2). Photons with energies of 10.49 eV can ionize all isomers; 10.20 eV photons may ionize all isomers except 1-eclipsedmethoxymethanol, whereas 9.40 eV photons only ionize dimethyl peroxide; 9.00 eV photons cannot ionize either isomer. Since the precursor CD<sub>3</sub>OH has an IE of  $10.83 \pm 0.02 \, \text{eV}$ (Person & Nicole 1971), it cannot be observed at the exploited photon energies. Considering the results, the overall ion counts decrease as the PI energies are lowered from 10.49 to 9.00 eV because the PI cross sections of the molecules decrease as the photon energies are reduced, and some pf the isomers cannot be ionized as the photon energy is lowered. Figure 3 presents the TPD profiles of mass-to-charge ratios critical to the present study: m/z = 68, 67, and 66.

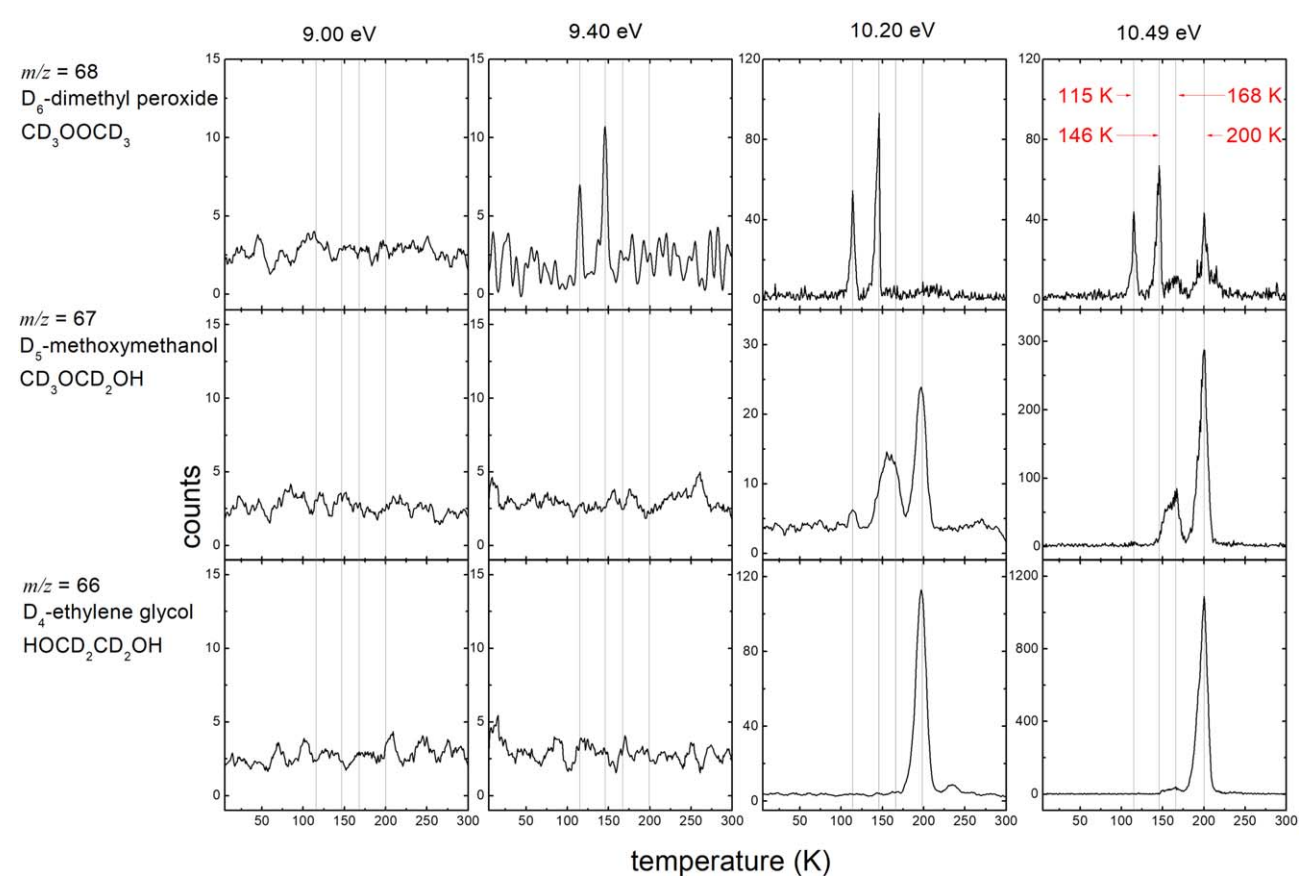


Figure 3. TPD traces for the different m/z-ratios assigned to the C<sub>2</sub>H<sub>6</sub>O<sub>2</sub> isomers at various deuteration levels.

$$4.2.1. \text{ m/z} = 68$$

Neutral species with a molecular weight of 68 amu bearing carbon, hydrogen, and/or deuterium, and oxygen can be linked to  $D_6$  substituted  $C_2H_6O_2$  isomers (Table 2) as well as  $D_8$ substituted C<sub>3</sub>H<sub>8</sub>O isomers (ethyl methyl ether (CD<sub>3</sub>OCD<sub>2</sub>CD<sub>3</sub>),  $IE = 9.72 \pm 0.07 \,\text{eV}$ ; 1-propanol (CD<sub>3</sub>CD<sub>2</sub>CD<sub>2</sub>OD), IE = $10.22 \pm 0.06 \, \text{eV}$ ; 2-propanol ((CD<sub>3</sub>)<sub>2</sub>CDOD), IE = 10.17 ± 0.02 eV; Bowen & Maccoll 1984; Koizumi et al. 1988). At a photon energy of 10.49 eV, four sublimation events at 115, 146, 168, and 200 K are detected, which can only be assigned to C<sub>2</sub>D<sub>6</sub>O<sub>2</sub> isomers, but not to C<sub>3</sub>D<sub>8</sub>O isomers as only one weak peak of  $C_3H_8^{18}O$  (m/z = 62) was observed at 124 K in the TPD phase of energetic electrons processed <sup>18</sup>O-methanol (CH<sub>3</sub><sup>18</sup>OH) ices under otherwise identical experimental conditions (Maity et al. 2015). By decreasing the photon energy to 10.20 eV, the peaks at 168 and 200 K vanish, thus attributing these events to D<sub>6</sub>-1-eclipsed-methoxymethanol (Table 2). Note that the electric field of the extractor plate lowers the ionization energy by up to 0.03 eV. The two sublimation events at 115 and 146 K are still clearly visible. The peaks at 115 K and 146 K are present at a photon energy of 9.40 eV, as well suggesting that they can only be associated to D<sub>6</sub>-dimethyl peroxide, which has an IE of 9.31 eV. Within the error limits, the ratios of the integrated areas of the ion counts of both sublimation events is constant at 9.40, 10.20, and 10.49 eV suggesting that both sublimation events originate from the same molecule, D<sub>6</sub>-dimethyl peroxide. At a photon energy of 9.00 eV, none of the isomers can be ionized (Figure 3). In summary, the data at m/z = 68 reveal the

formation of at least  $D_6$ -dimethyl peroxide ( $CD_3OOCD_3$ ) as well as  $D_6$ -1-eclipsed-methoxymethanol ( $CD_3OCD_2OD$ ).

$$4.2.2. \text{ m/z} = 67$$

The signal at m/z = 67 can be associated with D<sub>5</sub> substituted C<sub>2</sub>H<sub>6</sub>O<sub>2</sub> isomers. At a photon energy of 10.49 eV, three desorption events are detected: a weak peak at 115 K, a peak at 168 K with a shoulder at 155 K, and an intense sharp peak at 200 K (Figure 3). When the photon energy is lowered to 10.20 eV, all three sublimation events are still present. The signal at 10.20 eV cannot be attributed to D<sub>5</sub> substituted 1-eclipsed-methoxymethanol since its adiabatic ionization energy is higher, at 10.29 eV. However, the relative peak areas of the sublimation events at 168 K and 200 K at the 10.20 eV and  $10.49\,\mathrm{eV}$  experiments change from  $0.18\pm0.02$  to  $0.09 \pm 0.01$ , revealing that at least two isomers must be present at 10.49 eV. Lowering the photon energy to 9.40 eV eliminates all sublimation events. At 9.40 eV, D<sub>5</sub>-dimethyl peroxide should be ionized if present, but no ion counts are visible; hence, this isomer can be eliminated as a contributor to the sublimation events at 115, 155, and 168, and 200 K. Consequently, only D5-methoxymethanol and D5-ethylene glycol can account for the sublimation events.

$$4.2.3. \text{ m/z} = 66$$

Signals at m/z = 66 can originate from  $D_4$ -substituted  $C_2H_6O_2$  isomers. Two sublimation events at 168 K and 200 K are detected with 10.49 eV photons and vanish at a

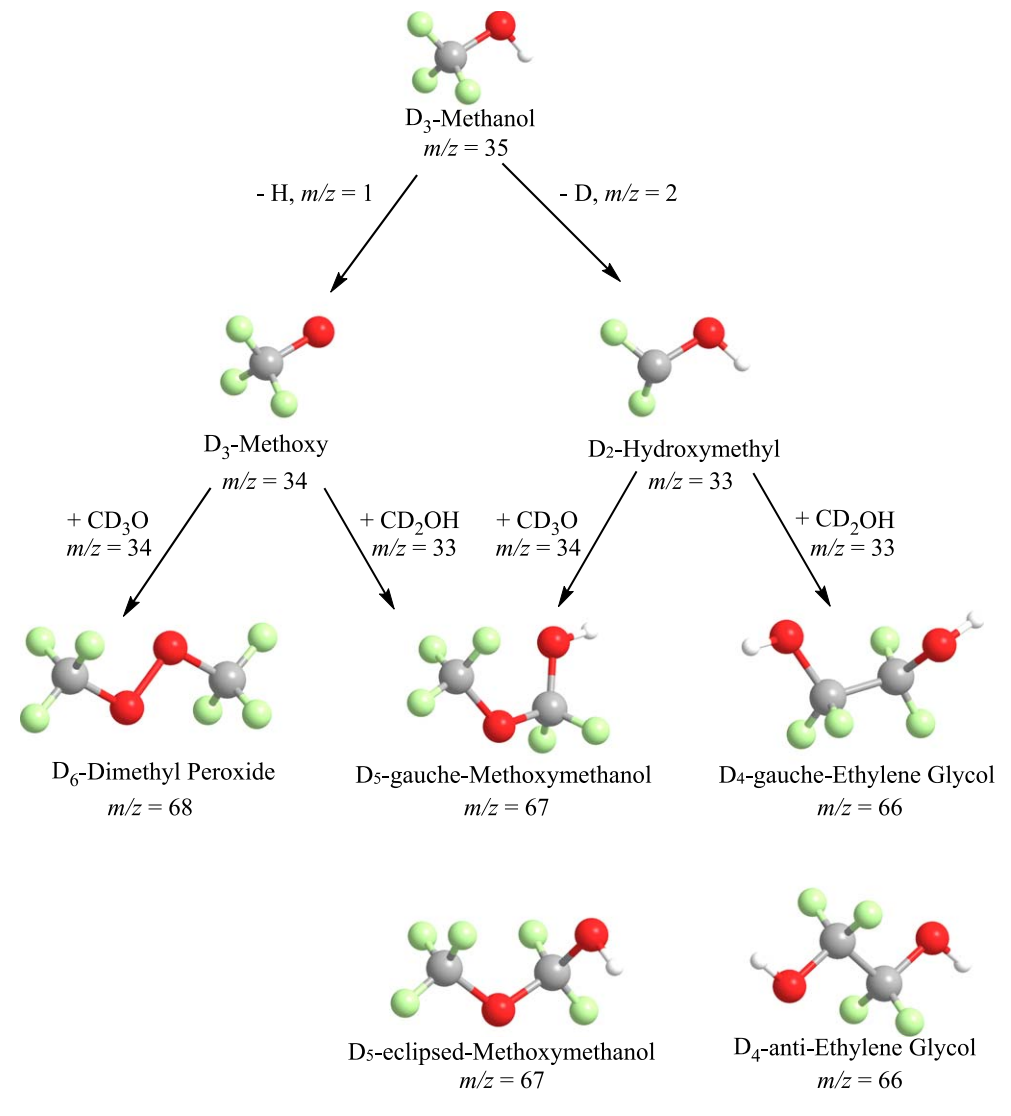


Figure 4. Reaction pathway toward distinct C<sub>2</sub>H<sub>6</sub>O<sub>2</sub> isomers at different deuteration levels.

photon energy of  $10.20\,\text{eV}$  (168 K event) and  $9.40\,\text{eV}$  (200 K event), respectively (Figure 3). Therefore, considering the IE, the sublimation event at  $168\,\text{K}$  has to be linked to  $D_4$ -1-eclipsed-methoxymethanol, whereas the  $200\,\text{K}$  event is associated with at least  $D_4$ -ethylene glycol.

# 4.2.4. *Isomers*

Overall, three isomers—dimethyl peroxide, methoxymethanol, and ethylene glycol at various degrees of deuteration—are synthesized and detected in the energetic electrons processed CD<sub>3</sub>OH ices with sublimation temperatures of 115 K and 146 K, 155 K and 168 K, and 200 K, respectively. Accounting for the aforementioned results, the sublimation events at 115 K and 146 K can be predominantly associated with the formation of D<sub>6</sub>-dimethyl peroxide (m/z = 68) and to a minor amount to co-subliming D<sub>5</sub>-methoxymethanol (m/z = 67). The sublimation peaks at 155 K and 168 K can be attributed to D<sub>6</sub>-/D<sub>5</sub>-/D<sub>4</sub>-methoxymethanol (m/z = 68, 67, and 66). Finally, the sublimation event at 200 K can be associated predominantly with D<sub>4</sub>-ethylene glycol (m/z = 66) with smaller amounts of D<sub>5</sub>-ethylene glycol (m/z = 67)

and co-subliming  $D_6$ -methoxymethanol (m/z = 68). Note that the sublimation temperature of ethylene glycol was previously determined to be 200 K thus verifying the aforementioned assignment of the dominating component of the 200 K event. Further, the room temperature boiling points of dimethyl peroxide, methoxymethanol, and ethylene glycol are 287, 356, and 470 K at atmospheric pressure (Rieche & Brumshagen 1928; Du et al. 2008; Bergantini et al. 2018a). This sequence can be correlated with an enhanced polarity and increased number of hydroxyl groups (OH), which can form hydrogen bonds, thus supporting our finding of the least polar dimethyl peroxide contributing to the sublimation event at the lowest temperature of 115 K with methoxymethanol and ethylene glycol found to dominate at 168 K and 200 K, respectively. Note that the sublimation temperature of pure methanol is 145 K and hence close to the sublimation events at 146 and 155 K of the irradiated CD<sub>3</sub>OH ices.

## 5. Discussion

Having confirmed the detection of methoxymethanol and its isomers, dimethyl peroxide and ethylene glycol, at various

Sublimation Events Photon Energy (eV) Mass-to-Charge Ratio (m/z) 115 K 146 K 168-155 K 200 K 10.49  $262 \pm 30$  $442\,\pm\,40$  $102\,\pm\,10$  $475\,\pm\,50$ 68 67  $37\,\pm\,4$  $1284 \pm 100$  $3359\,\pm\,300$  $350\,\pm\,40$  $13646 \pm 1000$ 66 10.20  $317 \pm 30$ 68  $469\,\pm\,50$ 67  $22 \pm 2$  $237 \pm 20$  $286 \pm 30$ 66  $1683\,\pm\,200$ 9.40 68  $49\,\pm\,5$  $74 \pm 10$ . . . . . . 67 66

 Table 4

 Integrated Peak Areas for All Sublimation Events

deuteration levels in the  $CD_3OH$  ices exposed to ionizing radiation, we now attempt to elucidate the reaction mechanisms involved in the generation of these species. Upon interaction of energetic electrons,  $CD_3OH$  undergoes unimolecular decomposition to  $D_3$ -methoxy ( $CD_3O$ ) radical with a suprathermal hydrogen atom (reaction 7) and to a  $D_2$ -hydroxymethyl ( $CD_2OH$ ) radical with a deuterium atom (reaction 8; Figure 4; Bennett et al. 2007):

$$CD_3OH \rightarrow CD_3O + H$$
 (7)

$$CD_3OH \rightarrow CD_2OH + D.$$
 (8)

The CD<sub>3</sub>O and CD<sub>2</sub>OH radicals produced in these processes are the "primary" radicals. These "primary" radicals may undergo three barrier-less radical–radical recombination reactions (9), (10), and (11) producing D<sub>6</sub>-dimethyl peroxide (68 amu), D<sub>5</sub>-methoxymethanol (67 amu), and D<sub>4</sub>-ethylene glycol 66 amu), respectively (Figure 4). Therefore, these reaction mechanisms account nicely for the ion counts of m/z = 68 (D<sub>6</sub>-dimethyl peroxide) at 115 K/146 K, of m/z = 67 (D<sub>5</sub>-methoxymethanol) at 115 K/155 K/168 K/200 K, and of m/z = 66 (D<sub>4</sub>-ethylene glycol) at 200 K with dominating contributions indicated in italics (Figure 4).

$$CD_3O + CD_3O \rightarrow CD_3OOCD_3$$
 (D<sub>6</sub>-dimethyl peroxide) (9)

$$CD_3O + CD_2OH \rightarrow CD_3OCD_2OH (D_5\text{-methoxymethanol})$$
(10)

$$CD_2OH + CD_2OH \rightarrow HOCD_2CD_2OH$$
 (D<sub>4</sub>-ethylene glycol). (11)

However, these reaction pathways cannot account for the detection of  $D_6$ -/ $D_4$ -methoxymethanol (m/z = 68 and 66;  $168 \, \text{K}$ ) and  $D_5$ -ethylene glycol (m/z = 67;  $200 \, \text{K}$ ). As the radiolysis proceeds and the concentration of hydrogen and deuterium atoms in the ice increases, the "primary" radicals may undergo atom-radical recombination forming  $D_4$ -methanol ( $CD_3OD$ ) (reaction 12) and  $D_2$ -methanol ( $CD_2HOH$ ) molecules (reaction 13)

$$CD_3O + D \rightarrow CD_3OD$$
 (12)

$$CD_2OH + H \rightarrow CD_2HOH.$$
 (13)

These molecules— $CD_3OD$  and  $CD_2HOH$ —can be decomposed by energetic electrons to the "primary" radicals (back reactions of reactions (12) and (13)) but also to  $D_3$ -hydroxymethyl ( $CD_2OD$ ; reaction 14) and  $D_2$ -methoxy ( $CD_2HO$ ) (reaction(15) radicals, which are labeled as "secondary" radicals.

$$CD_3OD \rightarrow CD_2OD + D$$
 (14)

$$CD_2HOH \rightarrow CD_2HO + H.$$
 (15)

These "secondary" radicals (CD<sub>2</sub>HO and CD<sub>2</sub>OD) may recombine with the previously mentioned "primary" radicals (CD<sub>3</sub>O and CD<sub>2</sub>OH) producing D<sub>5</sub>-dimethyl peroxide (reaction 16), D<sub>4</sub>-methoxymethanol (reaction 17), D<sub>6</sub>-methoxymethanol (reaction 18), and D<sub>5</sub>-ethylene glycol (reaction 19) or recombine with themselves generating D<sub>4</sub>-dimethyl peroxide (reaction 20), D<sub>5</sub>-methoxymethanol (reaction 21), and D<sub>6</sub>-ethylene glycol (reaction 22).

$$CD_2HO + CD_3O \rightarrow CD_2HOOCD_3$$
 (D<sub>5</sub>-dimethyl peroxide) (16)

$$CD_2HO + CD_2OH \rightarrow CD_2HOCD_2OH (D_4$$
-methoxymethanol) (17)

$$CD_2OD + CD_3O \rightarrow CD_3OCD_2OD (D_6\text{-methoxymethanol})$$
 (18)

$$CD_2OD + CD_2OH \rightarrow HOCD_2CD_2OD \ (D_5\text{-ethylene glycol}) \eqno(19)$$

$$CD_2HO + CD_2HO \rightarrow CD_2HOOCD_2H$$
 (D<sub>4</sub>-dimethyl peroxide) (20)

$$\label{eq:cd2} \begin{split} \text{CD}_2\text{HO} + \text{CD}_2\text{OD} &\rightarrow \text{CD}_2\text{HOCD}_2\text{OD} \text{ (D}_5\text{-methoxymethanol)} \\ &\qquad \qquad (21) \end{split}$$

$$\label{eq:cdot} \begin{split} CD_2OD + CD_2OD & \rightarrow DOCD_2CD_2OD \; (D_6\text{-ethylene glycol}). \end{split}$$

Considering the experimental detection of at least  $D_6$ - $/D_4$ -methoxymethanol (m/z = 68 and 66; 168 K) and  $D_5$ -ethylene glycol (m/z = 67; 200 K) at a level of typically less than 35% and 25% of  $D_5$ -methoxymethanol (m/z = 67; 168 K) and  $D_4$ -ethylene glycol (m/z = 66; 200 K), respectively (Table 4),

the presence of reactions (17)–(19) is required to account for the experimental data thus highlighting the role of hydrogen—deuterium exchanges at elevated radiation doses.

# 6. Astrophysical Implications

In this study, by using tunable PI-ReTOF-MS, we elucidated the formation pathways of methoxymethanol (CH<sub>3</sub>OCH<sub>2</sub>OH) and its structural isomers ethylene glycol (HOCH<sub>2</sub>CH<sub>2</sub>OH) and dimethyl peroxide (CH<sub>3</sub>OOCH<sub>3</sub>) at various levels of deuteration at 5 K under the influence of ionizing radiation at radiation doses of interstellar ices equivalent to about 15 million years of exposure to GCRs inside a prototype molecular cloud (Yeghikyan 2011; Bergantini et al. 2018a). These results imply that CH<sub>3</sub>OH could represent a critical precursor for the detected CH<sub>3</sub>OCH<sub>2</sub>OH (McGuire et al. 2017) and HOCH<sub>2</sub>CH<sub>2</sub>OH (Hollis et al. 2002; Brouillet et al. 2015; Rivilla et al. 2017), which may be generated via radical-radical reactions within interstellar ices, in distinct low temperature interstellar environments. The spatial distributions analysis of COMs in the MM1 and MM2 cores in the high-mass star-forming region NGC 6334I reveals that the distribution of CH<sub>3</sub>OCH<sub>2</sub>OH is notably similar to that of the potential CH<sub>3</sub>OH precursor, supporting that methanol represents a possible critical precursor molecule of CH<sub>3</sub>OCH<sub>2</sub>OH. The emission from HOCH<sub>2</sub>CH<sub>2</sub>OH is more compact compared to CH<sub>3</sub>OCH<sub>2</sub>OH. This difference has also been found in other star-forming regions such as G31.41+0.31 (Rivilla et al. 2017) and is likely due to line opacity of this low abundance species. Finally, this is the first unambiguous synthesis and detection of CH<sub>3</sub>OOCH<sub>3</sub> as a radiolysis product of CH<sub>3</sub>OH. The sublimation event at about 120 K was detected during the TPD phase of irradiated CH<sub>3</sub>OH ice at  $PI = 10.49 \, eV$  (Maity et al. 2015) but was not confirmed to be CH<sub>3</sub>OOCH<sub>3</sub> by tuning down photon energies. It shall be stressed that previous studies (Allamandola et al. 1988; Gerakines et al. 1996; Öberg et al. 2009) failed to identify CH<sub>3</sub>OOCH<sub>3</sub> in irradiated methanol ices via infrared spectroscopy and/or mass spectrometry utilizing electron impact ionization of the subliming molecules, thus demonstrating the unique power of PI-ReTOF-MS to identify truly complex and reactive organics in space simulation experiments. Given the detection of hitherto unobserved interstellar CH<sub>3</sub>OOCH<sub>3</sub> in this study, it is reasonable to expect future observations of this still elusive molecule in methanol-rich star-forming regions, such as W33A, IRAS 03301+3111, NGC 1068, and RAFGL 7009S (Dartois et al. 1999; van der Tak et al. 2000; Boogert et al. 2008; Tosaki et al. 2017).

The Hawaii group acknowledges support from the US National Science Foundation, Division of Astronomical Sciences under grant AST-1800975. The equipment was financed by the W. M. Keck Foundation. R.C.F. acknowledges support from NASA grant NNX17AH15G, NSF Grant OIA-1757220, and start-up funds provided by the University of Mississippi.

# Appendix

Figure 5 shows the PI-ReTOF-MS spectra of the subliming molecules from unirradiated CD<sub>3</sub>OH ices recorded at photon energy of 10.49 eV. No signal was detected.

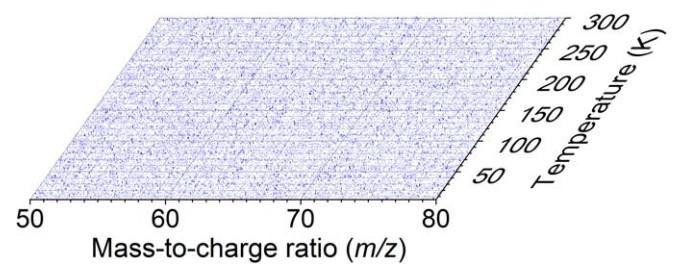


**Figure 5.** PI-ReTOF-MS spectra of the subliming molecules from unirradiated CD<sub>3</sub>OH ices recorded at photon energy of 10.49 eV.

### **ORCID iDs**

Cheng Zhu https://orcid.org/0000-0002-7256-672X Alexandre Bergantini https://orcid.org/0000-0003-2279-166X

Ryan C. Fortenberry https://orcid.org/0000-0003-4716-8225

Ralf I. Kaiser https://orcid.org/0000-0002-7233-7206

#### References

Abplanalp, M. J., Förstel, M., & Kaiser, R. I. 2016a, CPL, 644, 79 Abplanalp, M. J., Gozem, S., Krylov, A. I., et al. 2016b, PNAS, 113, 7727 Allamandola, L., Sandford, S., & Valero, G. 1988, Icar, 76, 225 Ball, J. A., Gottlieb, C. A., Lilley, A., & Radford, H. 1970, ApJL, 162, L203 Becke, A. D. 1993, JChPh, 98, 5648 Bennett, C. J., Chen, S.-H., Sun, B.-J., Chang, A. H., & Kaiser, R. I. 2007, ApJ, 660, 1588 Bennett, C. J., Hama, T., Kim, Y. S., Kawasaki, M., & Kaiser, R. I. 2010, ApJ, 727, 27 Bennett, C. J., Jamieson, C. S., Osamura, Y., & Kaiser, R. I. 2005a, ApJ, 624, 1097 Bennett, C. J., & Kaiser, R. I. 2007a, ApJ, 660, 1289 Bennett, C. J., & Kaiser, R. I. 2007b, ApJ, 661, 899 Bennett, C. J., Osamura, Y., Lebar, M. D., & Kaiser, R. I. 2005b, ApJ, 634, 698 Bergantini, A., Góbi, S., Abplanalp, M. J., & Kaiser, R. I. 2018a, ApJ, 852, 70 Bergantini, A., Maksyutenko, P., & Kaiser, R. I. 2017, ApJ, 841, 96 Bergantini, A., Zhu, C., & Kaiser, R. I. 2018b, ApJ, 862, 140 Boamah, M. D., Sullivan, K. K., Shulenberger, K. E., et al. 2014, FaDi, 168, 249 Boogert, A. C., Pontoppidan, K. M., Knez, C., et al. 2008, ApJ, 678, 985 Boogert, A. C. A., Gerakines, P. A., & Whittet, D. C. B. 2015, ARA&A, Bouilloud, M., Fray, N., Benilan, Y., et al. 2015, MNRAS, 451, 2145 Bowen, R. D., & Maccoll, A. 1984, OrMSp, 19, 379 Boyer, M. C., Boamah, M. D., Sullivan, K. K., et al. 2014, JPCC, 118, 22592 Brouillet, N., Despois, D., Lu, X.-H., et al. 2015, A&A, 576, A129 Brown, R., Crofts, J., Gardner, F., et al. 1975, ApJL, 197, L29 Crawford, T. D., & Schaefer, H. F., III 2000, in Reviews in Computational Chemistry, ed. K. B. L. D. B. Boyd (New York: Wiley), 33 Dartois, E., Schutte, W., Geballe, T., et al. 1999, A&A, 342, L32 Drouin, D., Couture, A. R., Joly, D., et al. 2007, J. Scanning Microsc., 29, 92 Du, J. R., Chakma, A., & Feng, X. 2008, SPTe, 64, 63 Falk, M., & Whalley, E. 1961, JChPh, 34, 1554 Frigge, R., Zhu, C., Turner, A. M., et al. 2018, ChCom, 54, 10152 Frisch, M., Trucks, G., Schlegel, H., et al. 2009, Gaussian 09, Revision D. 01 (Wallingford, CT: Gaussian) Gerakines, P., Schutte, W., & Ehrenfreund, P. 1996, A&A, 312, 289 Gilmore, W., Morris, M., Johnson, D., et al. 1976, ApJ, 204, 43 Groner, P., Stolkin, I., & Gunthard, H. H. 1973, JPhE, 6, 122 Harris, T. D., Lee, D. H., Blumberg, M. Q., & Arumainayagam, C. R. 1995, JPhCh, 99, 9530 Hays, B. M., & Widicus Weaver, S. L. 2013, JPCA, 117, 7142 Hollis, J. M., Lovas, F. J., Jewell, P. R., & Coudert, L. 2002, ApJL, 571, L59 Howe, D., Millar, T., Schilke, P., & Walmsley, C. 1994, MNRAS, 267, 59 Huang, L., Asvany, O., Chang, A., et al. 2000, JChPh, 113, 8656

Huang, L., Lee, Y., & Kaiser, R. 1999, JChPh, 110, 7119

Jones, B. M., & Kaiser, R. I. 2013, J. Phys. Chem. Lett., 4, 1965

Huh, S. B., & Lee, J. S. 2003, JChPh, 118, 3035

```
Kaiser, R. I., Maksyutenko, P., Ennis, C., et al. 2010a, FaDi, 147, 429
Kaiser, R. I., Sun, B. J., Lin, H. M., et al. 2010b, ApJ, 719, 1884
Kawaguchi, K., Ohishi, M., Ishikawa, S.-I., & Kaifu, N. 1992a, ApJL,
  386, L51
Kawaguchi, K., Takano, S., Ohishi, M., et al. 1992b, ApJL, 396, L49
Kendall, R. A., Dunning, T. H., Jr, & Harrison, R. J. 1992, JChPh, 96, 6796
Koizumi, H., Shinsaka, K., Yoshimi, T., et al. 1988, IJRAI, 32, 111
Kostko, O., Zhou, J., Sun, B. J., et al. 2010, ApJ, 717, 674
Laas, J. C., Garrod, R. T., Herbst, E., & Weaver, S. L. W. 2011, ApJ, 728, 71
Lee, C., Yang, W., & Parr, R. G. 1988, PhRvB, 37, 785
Loison, J.-C., Agúndez, M., Marcelino, N., et al. 2016, MNRAS, 456, 4101
Loomis, R. A., McGuire, B. A., Shingledecker, C., et al. 2015, ApJ, 799, 34
Maity, S., Kaiser, R. I., & Jones, B. M. 2014, FaDi, 168, 485
Maity, S., Kaiser, R. I., & Jones, B. M. 2015, PCCP, 17, 3081
McGuire, B. A., Shingledecker, C. N., Willis, E. R., et al. 2017, ApJL, 851, L46
Mehringer, D. M., Snyder, L. E., Miao, Y., & Lovas, F. J. 1997, ApJL,
  480, L71
Motiyenko, R. A., Margulès, L., Despois, D., & Guillemin, J.-C. 2018, PCCP,
   20, 5509
Neill, J. L., Muckle, M. T., Zaleski, D. P., et al. 2012, ApJ, 755, 153
Öberg, K. I., Garrod, R. T., Van Dishoeck, E. F., & Linnartz, H. 2009, A&A,
Person, J. C., & Nicole, P. P. 1971, JChPh, 55, 3390
Peterson, K. A., & Dunning, T. H., Jr 1995, JChPh, 102, 2032
Raghavachari, K., Trucks, G. W., Pople, J. A., & Head-Gordon, M. 1989, CPL,
```

```
Rieche, A., & Brumshagen, W. 1928, BDCG, 61B, 951
Rivilla, V., Beltrán, M., Cesaroni, R., et al. 2017, A&A, 598, A59
Saenko, E. V., & Feldman, V. I. 2016, PCCP, 18, 32503
Schneider, H., Caldwell-Overdier, A., Coppieters 't Wallant, S., et al. 2019,
  MNRAS, 485, L19
Shu, J., Wilson, K. R., Ahmed, M., & Leone, S. R. 2006, RScI, 77, 043106
Snyder, L., Buhl, D., Schwartz, P., et al. 1974, ApJL, 191, L79
Socrates, G. 2004, Infrared and Raman Characteristic Group Frequencies (3rd
  ed.; New York: Wiley)
Sullivan, K. K., Boamah, M. D., Shulenberger, K. E., et al. 2016, MNRAS,
Tosaki, T., Kohno, K., Harada, N., et al. 2017, PASJ, 69, 18
Turner, A. M., Abplanalp, M. J., Chen, S. Y., et al. 2015, PCCP, 17, 27281
Turner, A. M., Bergantini, A., Abplanalp, M. J., et al. 2018, NatCo, 9, 3851
Turner, B. 1971, ApJL, 163, L35
Turner, B. E., & Apponi, A. J. 2001, ApJL, 561, L207
van der Tak, F. F. S., van Dishoeck, E. F., & Caselli, P. 2000, A&A, 361, 327
Werner, H., Knowles, P., Knizia, G., et al. 2015, MOLPRO, Version 2015.1, a
  Package of ab Initio Programs, http://www.molpro.net
Werner, H. J., Knowles, P. J., Knizia, G., Manby, F. R., & Schütz, M. 2012,
      ley Interdiscip. Rev.: Comput. Mol. Sci., 2, 242
Wilson, K. R., Jimenez-Cruz, M., Nicolas, C., et al. 2006, JPCA, 110, 2106
Xue, C., Remijan, A. J., Burkhardt, A. M., & Herbst, E. 2019, ApJ, 871, 112
Yang, W., Parr, R. G., & Lee, C. 1986, PhRvA, 34, 4586
Yeghikyan, A. 2011, Ap, 54, 87
Zhu, C., Frigge, R., Turner, A. M., et al. 2018, ChCom, 54, 5716
```